

Marcus V. G. Muniz¹, J Allan A. Lyrio¹ & João Luiz F. Azevedo²

¹Instituto Tecnológico de Aeronáutica, 12228-900, São José dos Campos - SP, Brazil
 ²Instituto de Aeronáutica e Espaço, 12228-904, São José dos Campos - SP, Brazil

Abstract

The present work employs linear system techniques for the identification of aerodynamic loads over an airfoil with a control surface subject to unsteady airflow at transonic Mach number. The response of the aeroelastic system inputs in pitch, plunge and control surface degrees of freedom are computed by solving the unsteady Euler equations. The mesh displacement simulating the airfoil movement is imposed using Radial Basis Functions (RBFs) with compact support and compared against the rigid body movement for the plunge and pitch degrees of freedom. Discrete steps are used to displace the mesh and the transfer functions are obtained using the SIMO system identification methodology. As a preparation for the next steps of the research, open and closed loop flutter stability analyses at low Mach number are performed on a NACA0012 airfoil with three degrees of freedom. An optimal linear quadratic regulator (LQR) is designed to increase the flutter speed.

Keywords: Aeroservoelasticity, Unsteady Aerodynamics, System Identification, CFD

1. Introduction

Aeroservoelastic phenomena are complex interactions of the inertial, elastic and aerodynamic forces with the flight control systems of an aircraft which can lead to instabilities and induce a structural collapse. With the evolution of control systems theory and the emergence of digital computers in the mid-1960s, control laws were employed in the aircraft design to improve its flight dynamics characteristics [1]. In these early developments the aerodynamic loads were obtained from an extension of some form of the Generalized Theodosen's Function or Jones' approximation to Wagner's function to the three-dimensional case using, for instance, the strip theory [2]. One noticeable limitation of the this approach is that all the aerodynamic frequency response relations are dependent solely on the Theodorsen's function. As the aeroeslatic systems become more complex, it is unlikely that the transfer functions in all the degrees of freedom can be well modeled by only one impulse response function. Vepa [3] applied Padé's Approximats Matrices to enable different functions for each term in the aerodynamic influence matrix. Edwards [4] used these matrices to compute the flutter boundaries in a NACA0012 airfoil obtaining good results on the design of active flutter suppression control laws. rog [5] approximated the transfer functions employing Rational Function Approximationis (RFA) with fixed poles. Eversman and Tewari [6, 7] improved this approach by allowing variable poles in the RFAs, improving the approximation to the aerodynamic response.

An additional limitation arising by using the Theodorsen's function and its approximations to obtain the aerodynamic transfer functions resides in the fact that the solution is obtained from the potential flow theory, which does not account for viscosity or transonic effects. It was not until the 1970s with work from Jameson and Caughey [8] or Pulliam and Steger [9] that transonic flows described by the Euler equations of fluid dynamics were numerically solved.

In the authors' research group, Oliveira [10] first obtained the aerodynamic transfer functions of a typical section using an in-house developed Computational Fluid Dynamics (CFD) code, employing Eversman and Tewari's RFAs with variable poles. Linear Time Invariant (LTI) systems techniques

were employed to obtain the transfer functions in a Single Input - Multiple Output (SIMO) fashion moving the airfoil as a rigid body for both plunge and pitch degrees of freedom (DOF). Later, Marques and Azevedo [11] demonstrated that for very small displacements the response of the nonlinear Euler equations of motion (EOM) presents a linear behaviour warranting the application of LTI systems theory. This conclusion applies even for transonic Mach numbers. In that work the rigid body mesh movement approach was also compared with a spring analogy approach showing that the mesh motion introduced errors inviabilized the solution for the later. This is a significant limitation for aeroservoelastic analysis as relative displacements of the mesh are required to model the control surface movement. In the present work Radial Basis Functions (RBFs) are used to simulate the airfoil motion employing the methodology described in Lyrio et al. [12, 13]. A validation is performed against for the transfer functions due to pitch and plunge displacements presented in Oliveira [10]. The transfer functions due to a third degree of freedom are also computed, namely aerodynamic lift, pitching moment and hinge moment response to the displacement of trailing edge or control surface. As a preparation for the next step of the present research, a control law is designed to delay the flutter onset point of the three DOFs aeroelastic system in subsonic conditions with the aerodynamic response obtained by Edwards [4]. The root locus of both open and closed loop system are presented alongside a simulation of an initial disturbance on the airfoil angle of attack.

2. Theoretical Formulation

2.1 Aeroelastic Formulation

An aeroservoelastic analysis is performed on the three degrees of freedom typical section shown in Fig. 1. It is a two-dimensional representation of a wing section equipped with a control surface on the trailing edge. The typical section is connected to a linear actuator not shown in the figure. The actual control surface displacement relates to the system input by a linear function of the stiffness on actuation chain.

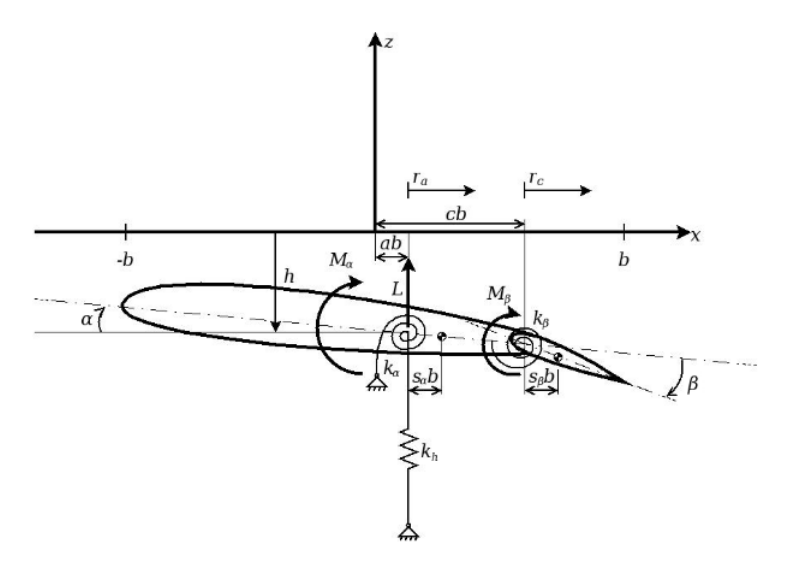


Figure 1 – Typical section with a control surface, adapted from [14].

The equations of motion of the aeroelastic system are given by

$$[M_S|\{\ddot{\eta}(t)\} + [K_S|\{\eta(t)\} = \{Qa(t)\} + \{G\}u(t), \tag{1}$$

where:

$$\{\eta\} = \begin{cases} \xi(t) \\ \alpha(t) \\ \beta(t) \end{cases},\tag{2}$$

is the vector whose components are the non dimensional generalized coordinates describing the displacements in both pitch (α) , plunge (ξ) and control surface deflection (β) degrees of freedom.

The generalized coordinate describing the displacement in plunge, ξ , is obtained by dividing the physical coordinate, h, by the typical section semi chord b, $\xi = h/b$.

$$[M_s] = \begin{bmatrix} 1 & \chi_{\alpha} & \chi_{\beta} \\ \chi_{\alpha} & r_{\alpha}^2 & r_{\beta}^2 + \chi_{\beta}(c-a) \\ \chi_{\beta} & r_{\beta}^2 + \chi_{\beta}(c-a) & r_{\beta}^2 \end{bmatrix}, \tag{3}$$

is the generalized structural mass matrix. It is described in terms of the dimensionless static unbalances, χ_{α} and χ_{β} , as well as the dimensionless radii of gyration, r_{α} and r_{β} . The dimensionless static unbalances are given by $\chi_{\alpha} = S_{\alpha}/mb$ and $\chi_{\beta} = S_{\beta}/m_{\rm CS}b$. $S_{\alpha} = mx_{a}b$ is the dimensional static unbalance of the typical setcion. It is function of m, the mass of the airfoil combined with the control surface, x_{a} the distance of the elastic axis to center of mass, and b the semi chord as shown if Fig 1. In the same sense $S_{\beta} = m_{\rm CS}x_{\beta}b$ is the dimensional static unbalance of the control surface, which is function of $m_{\rm CS}$, the mass of the control surface. The reader should note that the static unbalance of the control surface is also non-dimensionalized by the typical section semi-chord b. The dimensionless radius of gyration in pitch of the typical section is given by $r_{\alpha} = \sqrt{I_{\alpha}/mb^{2}}$, where I_{α} is moment of inertia of the typical section measured on the pitch axis passing through the center of mass. $r_{\beta} = \sqrt{I_{\beta}/m_{\rm CS}b^{2}}$ is the dimensionless radius of gyration of the control surface where I_{β} is moment of inertia of the control surface measured on the hinge line.

$$[K_s] = \begin{bmatrix} \omega_h & 0 & 0 \\ 0 & r_{\alpha}^2 \omega_{\alpha}^2 & 0 \\ 0 & 0 & r_{\beta}^2 \omega_{\beta}^2 \end{bmatrix}, \tag{4}$$

is the generalized stiffness structural matrix described in terms of the natural circular frequencies for the plunge, pitch and control surface rotational modes, $\omega_h = \sqrt{k_h/m}$, $\omega_\alpha = \sqrt{k_\alpha/I_\alpha}$, and $\omega_\beta = \sqrt{k_\beta/I_\beta}$, respectively. k_h is the stiffness of the typical section in the plunge structural mode, k_α is the stiffness in the pitch structural mode and k_β in the control surface structural mode. The vector containing the aerodynamic loads, i.e, lift force, pitch moment and hinge moment, is given by

$$\{Qa(t)\} = \begin{bmatrix} \frac{Qa_h(t)}{mb} \\ \frac{Qa_\alpha(t)}{mb^2} \\ \frac{Qa_\beta(t)}{mb^2} \end{bmatrix} . \tag{5}$$

The function u(t) is the control surface position commanded by the controller, whereas $\{G\}$ is the control input distribution vector which relates the applied hinge moment to the control surface position. The above equations are dimensionless in terms of the generalized displacements, however not with respect to time. In order to make them dimensionless also in terms of the time variable a reference circular frequency, ω_r , considered herein equal to ω_α , is used to obtain the non dimensional time variable $\bar{t} = t\omega_r$. Applying the chain rule on the time derivative, one gets the dimensionless form of the equations of motion, Eq. 1, as:

$$[M_s]\{\ddot{\eta}(\bar{t})\} + [\overline{K}]\{\eta(\bar{t})\} = \{\overline{Qa}(\bar{t})\} + \{G\}u(\bar{t}), \tag{6}$$

The generalized mass matrix and the control input distribution vector, $[M_s]$ and $\{G\}$ respectively, are the same as previously described as none of their terms are dependent on time whereas

$$|\overline{K}| = 1/\omega_r^2 |K| \tag{7}$$

and

$$\{\overline{Qa}(\overline{t})\} = 1/\omega_r^2 \{Qa(\overline{t})\}. \tag{8}$$

The aerodynamic lift force and pitch and hinge moments are obtained using the fluid mechanics Euler equations solved by a CFD code developed in the research group. The flow solver is based on a cell centred, finite volume scheme. The time marching scheme is a second-order accurate, 5-stage, explicit scheme. It does not include pre-conditioning schemes and its validation for transonic conditions

is presented in Azevedo [15], Marques and Azevedo [11] and Oliveira [10]. Marques and Azevedo [16] show that, as long as the analysis is restricted to small perturbations, the unsteady aerodynamic force and pitch moment can be assumed as linear functions of the displacements in pitch and plunge. This holds even at high Mach numbers, where the Euler equations have a strong nonlinear character. A study is performed in the present work showing that the same linearity assumption can be considered for the aerodynamic response to perturbations on the control surface angle. This context warrants the use of the well-developed linear time invariant (LTI) system theory to predict and simulate the behavior of the aeroelastic system applying the convolution operation. This operation is facilitated if performed in the frequency domain where it converts to a simple multiplication operation. In the frequency domain, the equations of motion, Eq. 6, are given by

$$\overline{s}^{2}[M_{s}]\{\ddot{\chi}(\overline{s})\} + [\overline{K}]\{\chi(\overline{s})\} = \overline{Qa}(\overline{s}) + \{G\}\mathscr{U}(\overline{s}), \tag{9}$$

where $\bar{s} = s/\omega_r$, is the non dimensional Laplace transform variable; $\chi(\bar{s})$ and $\mathscr{U}(\bar{s})$ are the Laplace transforms of the generalized coordinate and control input distribution vectors, respectively.

2.2 System Identification Techniques Applied to Aerodynamic Transfer Functions

Linear continuous time invariant (LTI) systems have the property that the response to impulsive excitations contains all information about the system and the response to every other input is obtained by the convolution integral [17]:

$$y(t) = h(t) * x(t) = \int_0^t H(\lambda)x(t - \lambda)d\lambda, \tag{10}$$

where $H(\lambda)$ the transfer function of the system, which is the response of the system to the Dirac delta function, or impulse function, applied to any of the system DOFs. As this function is the derivative of the Heaviside function, or step function, it can be shown that the transfer function can also be obtained applying a step excitation to the system's input. As discussed by Noll and Azevedo [16], the discretization process converts the continuous time aerodynamic EOMs to a discrete time system, which enables the usage of the discrete equivalent functions to the continuous excitations, namely unit sample (US) and discrete step (DS) functions. Muniz and Azevedo [18] showed that the DS input, given by

$$u[n] = \begin{cases} 0, & n \le 0, \\ 1, & n > 0. \end{cases}$$
 (11)

provides better results using the CFD code employed in this work at transonic Mach numbers. On a SIMO system, the transfer function obtained from the solution of a DS input is computed performing a Fourier Transform (\mathscr{F}) on the difference operator (Δ) applied to the solution of the aerodynamic coefficient of interest:

$$G[n] = \mathscr{F}(\Delta(S_{DS})) = \mathscr{F}(S_{DS}[n] - S_{DS}[n-1]), \qquad (12)$$

where S_{DS} is the array whose elements are the response of the aerodynamic coefficients. For the typical section analyzed in this work, the aerodynamic transfer function matrix reads then

$$\overline{Qa}(\overline{s}) = \begin{pmatrix}
\frac{C_L(\overline{s})}{\alpha(\overline{s})} & \frac{C_M(\overline{s})}{\alpha(\overline{s})} & \frac{C_H(\overline{s})}{\alpha(\overline{s})} \\
\frac{C_L(\overline{s})}{\xi(\overline{s})} & \frac{C_M(\overline{s})}{\xi(\overline{s})} & \frac{C_H(\overline{s})}{\xi(\overline{s})} \\
\frac{C_L(\overline{s})}{\beta(\overline{s})} & \frac{C_M(\overline{s})}{\beta(\overline{s})} & \frac{C_H(\overline{s})}{\beta(\overline{s})}
\end{pmatrix} .$$
(13)

2.3 Rational Function Approximation (RFA)

In order to solve the aeroelastic EOMs, the tabulated values of aerodynamic transfer functions obtained from the CFD solutions are approximated by rational functions. Vepa [3] proposed and Edwards [4] implemented Padé approximants to the aerodynamic transfer functions. rog [5] employed different poles on the rational terms which were further simplified by Eversman and Tewari [6] with

the removal of the Laplace variable on the numerator leading to the following RFA used in the present work,

$$Q_a = [P_0] + [P_1]s' + [P_2]s'^2 + \sum_{j=3}^{N} \frac{P_j}{s' + \gamma_{j-2}}.$$
(14)

The coefficients of the rational polynomial, P_j , the number of poles and the poles themselves are obtained by an optimized least-squares approximation method in which the nonlinear lag parameters, γ_j , are interactively evaluated by a Simplex Search Method [19]. The lag state variables for this RFA formulation are given by

$$\eta_a(s)_j = \frac{1}{s + U^* \gamma_i} \eta(s). \tag{15}$$

The dynamic and input matrices of the state space equations, Eq. 20, then become

$$\bar{A} = \begin{bmatrix} 0 & I & 0 \\ -M^{-1}K & -M^{-1}B & -\left(\frac{U}{b}\right)M^{-1}P_{N} \\ 0 & I & -\left(\frac{u}{b}\right)\gamma_{N}I \end{bmatrix}$$
(16)

and

$$\bar{B} = \begin{bmatrix} 0 & M_s^{-1}G & 0 \end{bmatrix}^T. \tag{17}$$

The sub-matrices M, B and K, elements of the matrix \bar{A} , are given by $M=M_s-\frac{1}{2}\rho b^2[P_2]$, $B=-\frac{1}{2}\rho bU[P_1]$ and $K=K_s-\frac{1}{2}\rho bU^2[P_0]$, whereas $[P_0]$, $[P_1]$, $[P_2]$, ..., $[P_N]$ are those defined accordingly to Eq. 14 and the optimized least-square method.

2.4 Radial Basis Function with Compact Support and Mesh Movement

Marques and Azevedo [11] presented a comparison of two mesh movements strategies, namely rigid body and spring analogy motions. It shows that the former provided adequate transfer functions. However, the latter could result in significantly larger numberical errors with the current flow solver, depending on the amount of perturbation resulting from the mesh motion. In the present work, the prescribed motions are obtained by the application of a Radial Basis Function (RBF) interpolation [12, 13, 20], given by

$$d(x) = \sum_{i=1}^{i=N} \alpha_i \phi(||x - x_i||),$$
(18)

where $d(\mathbf{x})$ is the displacement of a node at the location x and ϕ is the RBF. x_i is the location of the RBF center used to limit the nodes being repositioned to those lying within the range of the compact support radius, r_{sup} . The RBFs used in this work are the zero and second Wendland's functions [21],

Wendland's C0:
$$\phi(||x||) = (1 - ||x||)^2$$
. (19)

2.5 Control System and Aeroservoelasticity

The aeroservoelastic analysis considers the effect of a control system interacting with the typical section. Figure 2 shows an adaptation of the traditional Collar's diagram to represent this new element interacting with the inertial, elastic and aerodynamic forces characterizing the aeroservoelastic system.

Equation 1 does not completely describe the dynamics of the aeroservoelastic system as the controller logic is still absent in the formulation. The modern control theory tools employed in this work for the controller design require the system represented in the state space form. The controller and the aeroelastic system, or the plant, are combined in a feedback arrangement forming a closed loop system. A full feedback system is characterized by all the outputs of the plant feeding the controller. The outputs of the control loop, i.e. the control law, are the actual inputs to the plant. The state space equations for a generic closed loop linear time invariant (LTI) system are given by

$$\dot{x}_{p}(t) = \bar{A}x_{p}(t) + \bar{B}[-\bar{K}x_{p}(t)] = [\bar{A} - \bar{B}\bar{K}]x_{p}(t) y_{p}(t) = \bar{C}x_{p}(t).$$
(20)

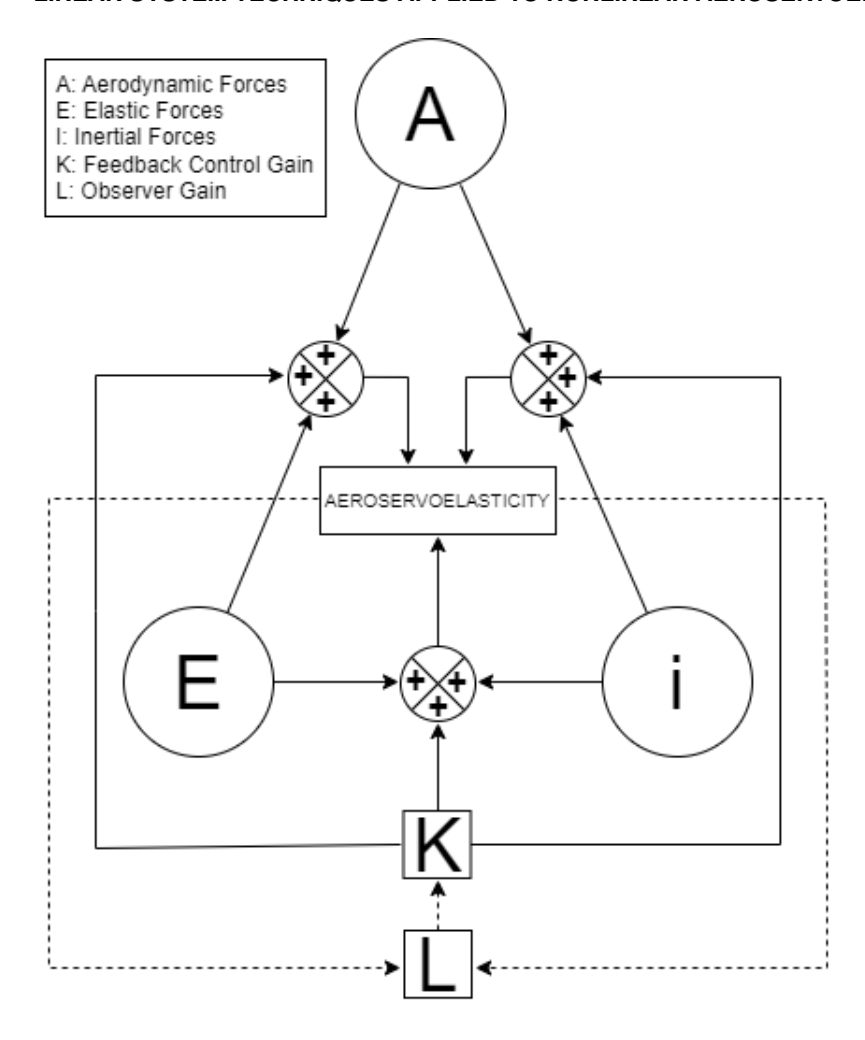


Figure 2 – Adaptation of the Collar's diagram by the authors to include the control system.

Equation 20 holds for a linear control law in the form $y_c = u_p = -[\bar{K}]x_p(t)$, where the sub-indices "p" and "c" stands for the plant and controller related variables, respectively. The y_c signal is the ouput of the controller which is fed as the input of the plant, u_p . The stability assessment is performed employing a root locus analysis on the system's poles obtained from the characteristic equation

$$\det\left(\left[\bar{A} - \bar{B}\bar{K}\right] - \lambda[I]\right) = 0, \tag{21}$$

where [I] is the identity matrix, and λ are the closed loop matrix eigenvalues. An appropriate choice of the gain matrix, $[\bar{K}]$, can place the poles at any desired location of the complex plane. In this work, an optimum Linear Quadratic Regulator is designed by minimizing the cost function

$$J = \frac{1}{2} \int_0^\infty \left(x^T(t) Q x(t) + u^T(t) R u(t) + 2x^T(t) N u(t) \right) dt.$$
 (22)

In this equation, Q is the state-cost weighted matrix, R is the input-cost weighted matrix and N the input-output cross matrix. The minimization procedure employs the "lqr" MATLAB® function to solve for S in the Riccati equation, given by:

$$\bar{A}^T S + S\bar{A} - (S\bar{B} + N)R^{-1}(\bar{B}^T S + N^T) + Q = 0.$$
(23)

The gain matrix K is then obtained using S as:

$$\bar{K} = R^{-1}(\bar{B}^T S + N^T)$$
 (24)

The solution algorithm is described in Arnold and Laub [22].

3. Results

In this section, the validation of the process to obtain the aerodynamic response of a NACA0012 airfoil at M=0.8 using RBF to execute the mesh displacements is presented. The assumption that the solution of the Euler equations can be represented by a linear superposition with regard to the modal motions, for small displacements, is also demonstrated for the control surface degree of freedom. The development of a control law to delay the flutter onset point is also demonstrated alongside the root-locus and time-domain simulations, after initial distrubances, to show the controller effectiveness.

3.1 RBF Validation

Muniz and Azevedo [18] demonstrated that the aerodynamic transfer functions due to pitch and plunge displacements of an NACA 0012 obtained with rigid mesh (RM) displacements are better identified using discrete steps to disturb the flow. The same approach is employed herein aiming at the validation of the calculation of the transfer functions using RBFs, including the displacements of the control surface. The aerodynamic response in this later case is obtained by the same CFD code, which was previously employed to compute aerodynamic transfer functions using a rigid body displacement of the grids, adapted to read the displaced mesh generated by a different code. A constant time step of 0.003 dimensionless time units is used, and the total simulation time is 300 dimensionless time units. The amplitudes of the pitch and plunge motions are $\alpha = 1. \times 10^{-4}$ deg. and $h = 1. \times 10^{-6}$ dimensionless length units, respectively. Marques and Azevedo [16] demonstrated the suitability of the linearity assumption that justifies the application of the LTI system theory for these step amplitudes. The radial basis function used to interpolate the mesh displacement is the C0 Wendland Function. Lyrio et al. [12] suggest that the supporting radius should be 0.3 < rsup/CMA < 1.10. Nonetheless, a supporting radius of $1. \times 10^{-2}$ nondimensional length units is used in this work. This lower value is more suitable for the current application as the displacements herein applied are much smaller than the ones employed in that work. An advantage of this approach is that it adds less numerical errors to the solution as the perturbations on the mesh are confined to a smaller region in space. Figure 3 illustrates the effect of moving the mesh and the control surface using the RBF approach for an step input. The size of the steps in this picture are exaggerated for clarity.

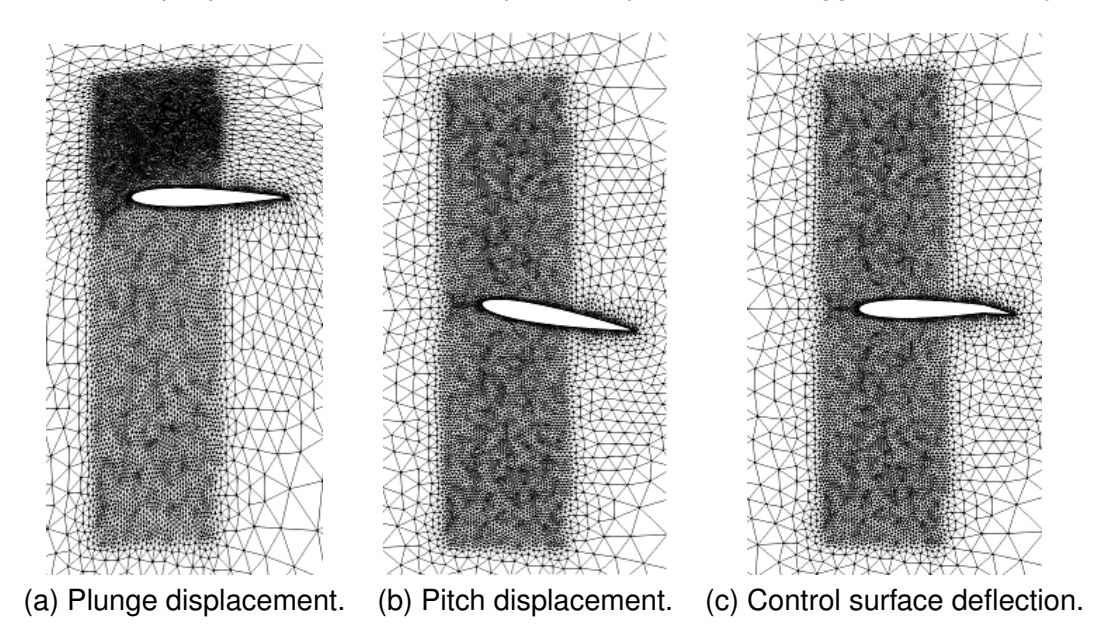


Figure 3 – NACA 0012 Airfoil Meshes - Exaggerated displacements showing the RBF effect.

Figure 4 presents the time histories of the lift and pitch moment coefficients for the airfoil subject to step inputs in pitch and plunge. Only the initial 0.1 dimensionless time units of the response are shown for clarity. The differences between the coefficients obtained from the simulations employing both the rigid body and RBF motion approaches are also shown. The errors are of the order of magnitude of 10^{-3} of the response in each case, *i.e.*, 0.1% of the corresponding coefficients. It shows that no relevant differences between the two approaches can be observed. Figure 5 shows the aerodynamic

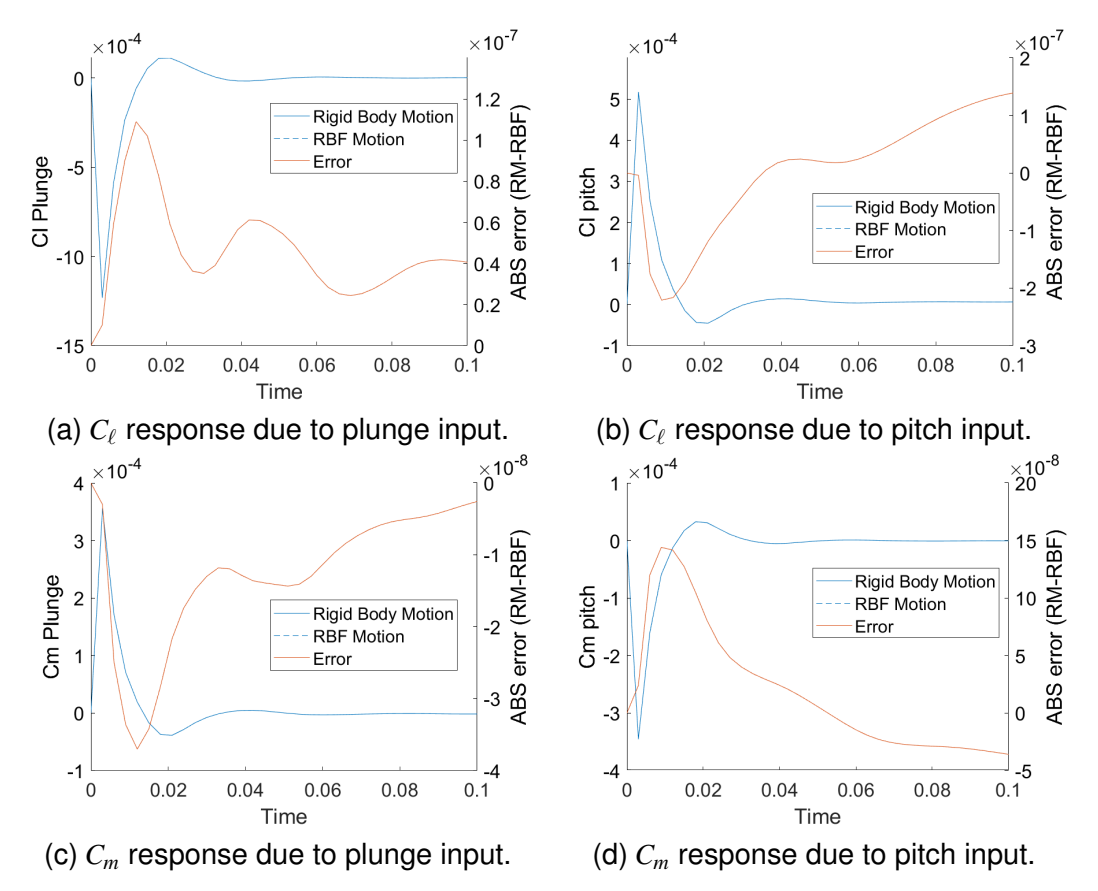


Figure 4 – Lift and pitching moment coefficient time histories, for calculations using RM and RBF, and the absolute error.

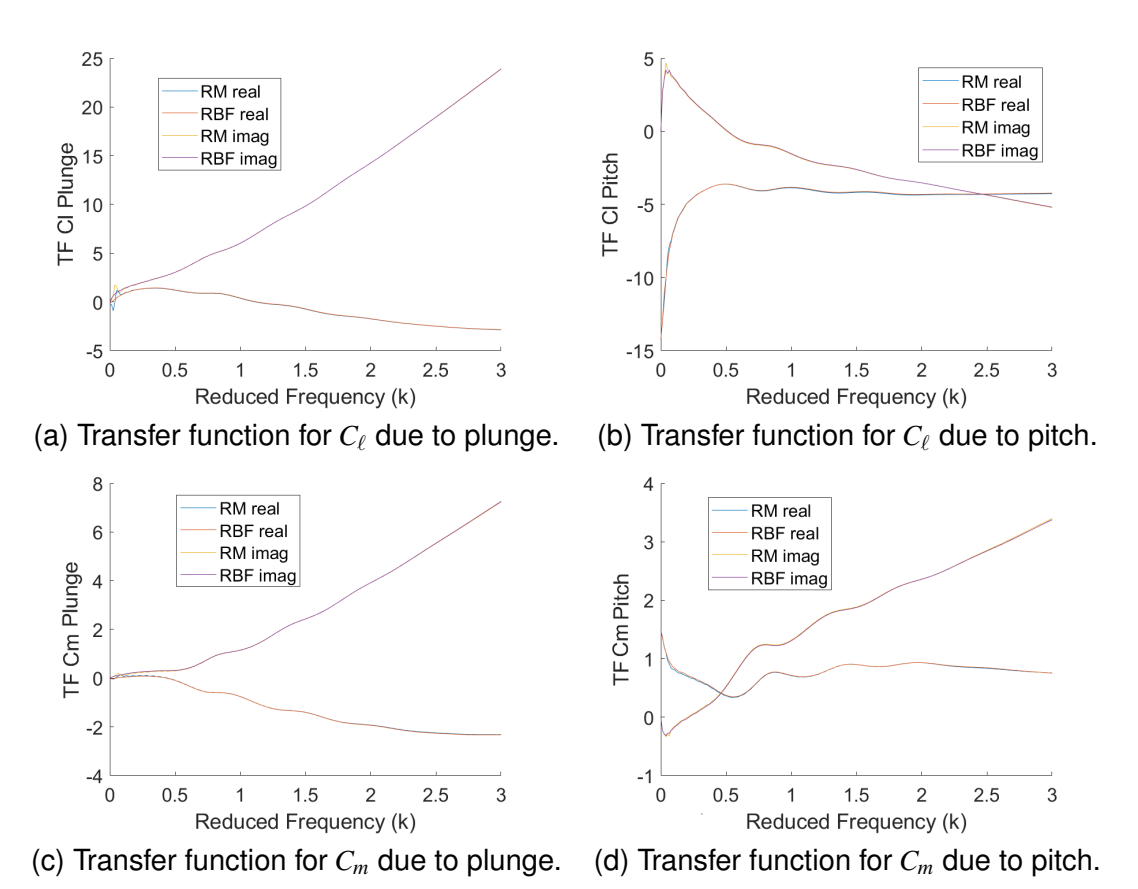


Figure 5 – Comparison of transfer functions obtained using RM vs RBF approaches.

transfer functions obtained from these same time histories. It is worth mentioning that there is a smoothing effect that the RBF mesh displacements bring to the data at very low frequencies. An enlarged view of the results in this low frequency range is shown in Fig. 6.

The results presented demonstrate the equivalence between obtaining the transfer functions using RBF or RM mesh motions. Furthermore, the validation presented herein shows not only the equivalence of both mesh displacements approaches, but it also demonstrates an improvement on the quality of the identified transfer functions for the RBF mesh motion due to the smoothing effect. The hinge moment coefficient (Chm) responses to both plunge and pitch inputs are presented in Fig. 7 for the RBF and RM mesh motions. The differences between the results obtained using both approaches are presented alongside the time histories. These differences are four orders of magnitude less than the coefficients themselves. Therefore, the results indicate errors of less than 0.01%. Figure 7 also shows the transfer functions of the hinge moment due to both plunge and pitch inputs. The smoothing effect at low reduced frequencies also appears on the hinge moment response. The plot evidencing this effect will not be shown here as it is similar to the one presented in Fig. 6. Therefore, the equivalence of the mesh motion approaches, RM and RBF, is also present in the hinge moment transfer functions due to pitch and plunge inputs.

3.2 Linearity Assumption for Flap Motion

An assessment of the linearity assumption regarding the input amplitude of the control surface is performed, similar to the one presented in Marques and Azevedo [16] for pitch and plunge inputs. Figure 8 shows the resulting transfer functions relating the aerodynamic coefficients due to control surface displacements for three step amplitudes, $\delta_{cs}=0.001$ deg., $\delta_{cs}=0.01$ deg. and $\delta_{cs}=0.5$ deg. The transfer functions match for the first and second deflections but not for the third one. This exercise demonstrates that 0.01 deg. is the limit for the linearity assumption and is the value assumed in the forthcoming analysis.

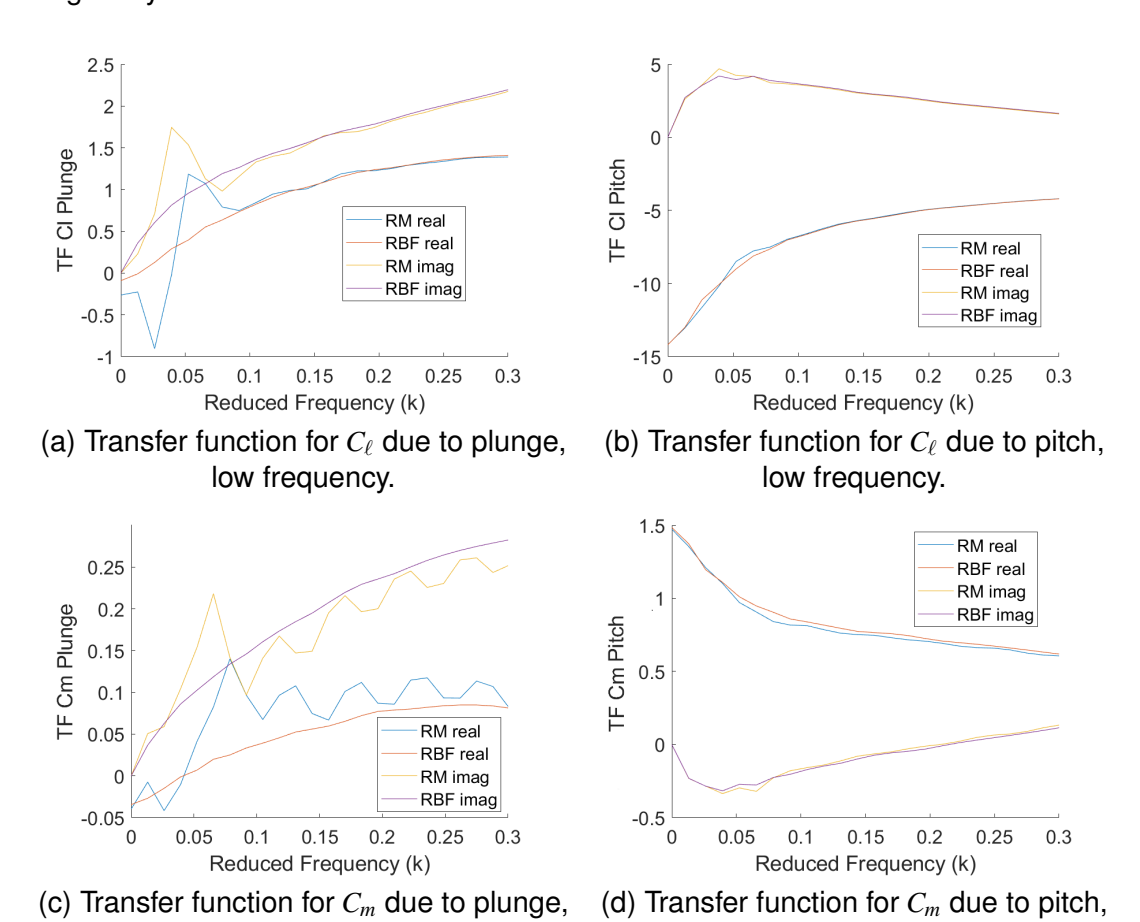
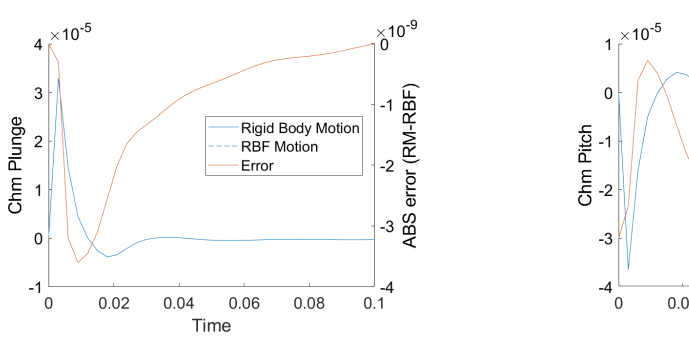
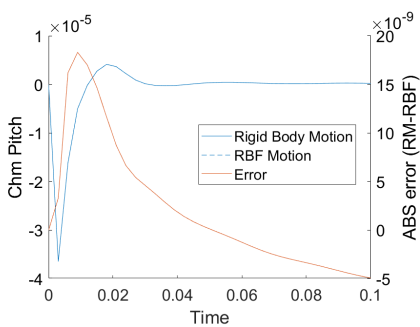


Figure 6 – Comparison of transfer functions obtained using the RM vs RBF approaches, in the low frequency range.

low frequency.

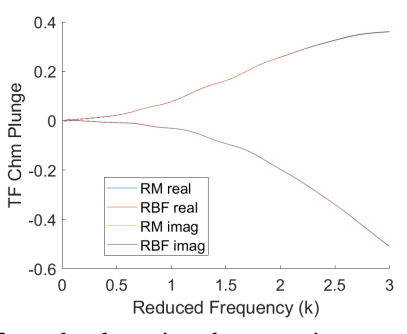
low frequency.

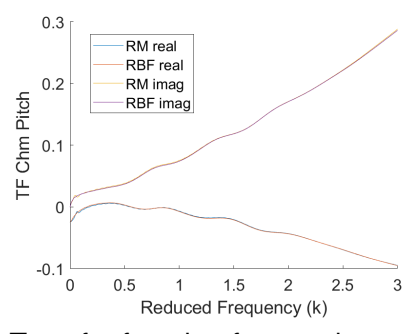




(a) Time history of C_{hm} due to plunge input.



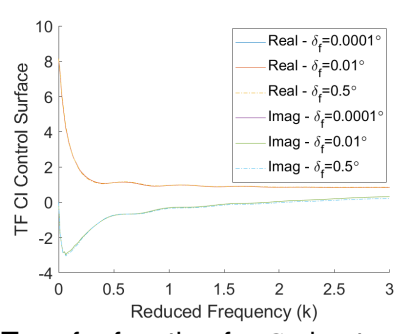


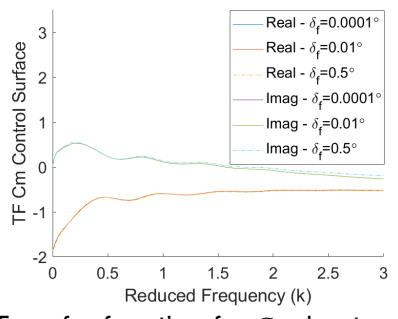


(c) Transfer function for C_{hm} due to plunge.

(d) Transfer function for C_{hm} due to pitch.

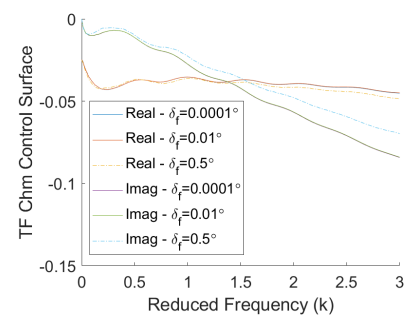
Figure 7 – Hinge moment coefficient time histories and transfer functions due to plunge and pitch inputs. Comparing results obtained using RM vs RBF.





(a) Transfer function for C_{ℓ} due to control surface deflection.

(b) Transfer function for C_m due to control surface deflection.



(c) Transfer function for C_{hm} due to control surface deflection.

Figure 8 – Transfer functions due to control surface deflection showing the effect of the input amplitude variation.

3.3 Subsonic Aeroservoelastic Analysis

The flow over the three degrees typical section at M = 0.2, also analyzed in this work, is well described by the potential flow theory. Aerodynamic transfer functions are obtained from the Theodorsen solution to the potential flow and harmonic oscillations, and extended to generic displacements by Jones

[23]. Aeroelastic analyses for both open and closed loop systems are performed on a typical section with the structural properties presented in Table 1.

Table 1 - Typica	I section	properties.
------------------	-----------	-------------

$\omega_{\alpha} = 100 \text{rad/sec}$	c = 0.6	$\zeta_{\alpha}=0$
$\omega_h = 50 \text{rad/sec}$	$\chi_{\alpha} = 0.2$	$\zeta_h = 0$
$\omega_{\beta} = 300 \text{rad/sec}$	$r_{\alpha}^{2} = 0.25$	$\zeta_{\beta} = 0$
$\mu = 40$	$\chi_{\beta} = 0.0125$	
a = -0.4	$r_{\beta}^2 = 0.00625$	

The open loop root locus analysis is presented in Fig. 9. It shows the flutter onset point at $U/b\omega_{\alpha}=2.99$. An optimal LQR controller is designed to delay the flutter onset point by minimizing the cost function shown in Eq. (22). In that equation, the components of the state-cost and input-output cross matrices, Q and N, are all set to zero. For the input-cost matrix, R, the identity matrix is assumed. The control is designed to delay the flutter onset point to $U/b\omega_{\alpha}=3.25$, which is set as the control law design point. However, as one can be see in the closed loop root locus also presented in Fig. 9, the flutter onset speed is actually raised to $U/b\omega_{\alpha}=3.65$.

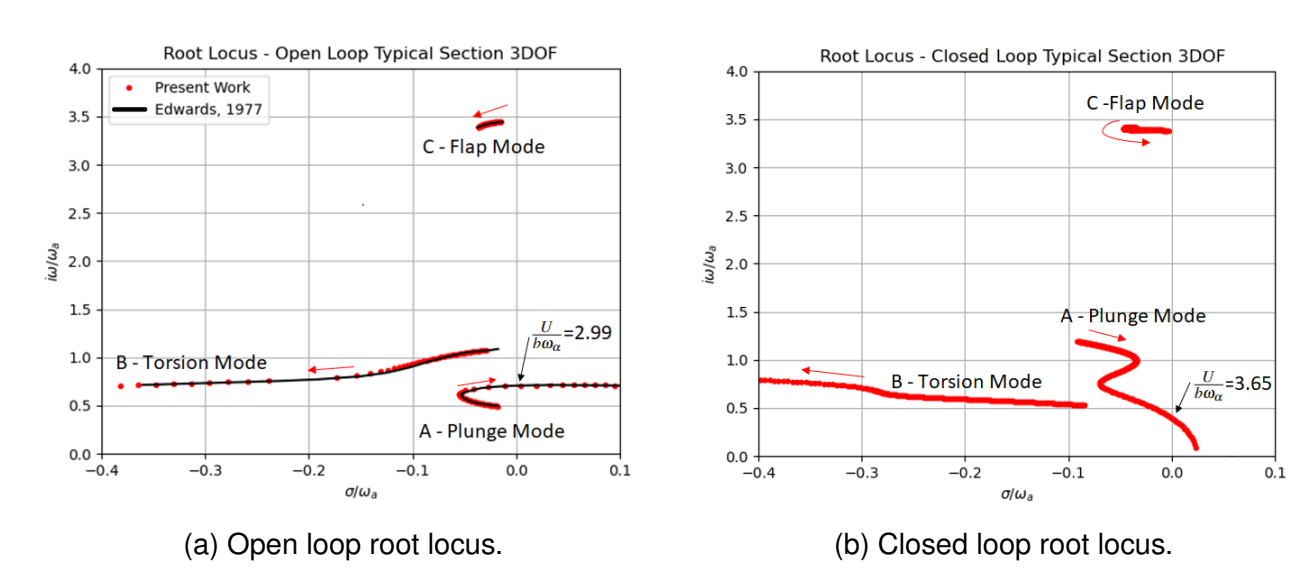
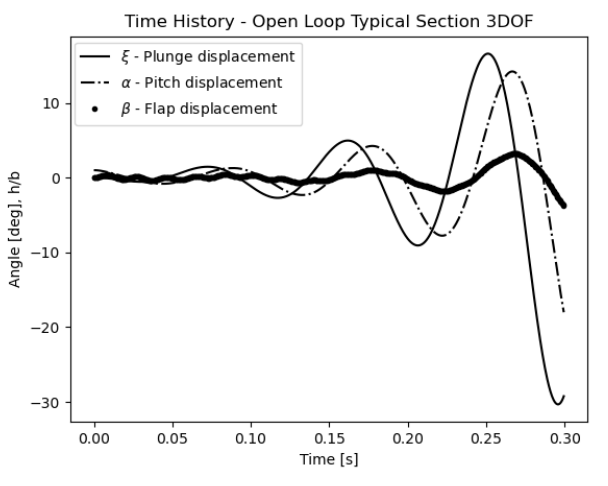


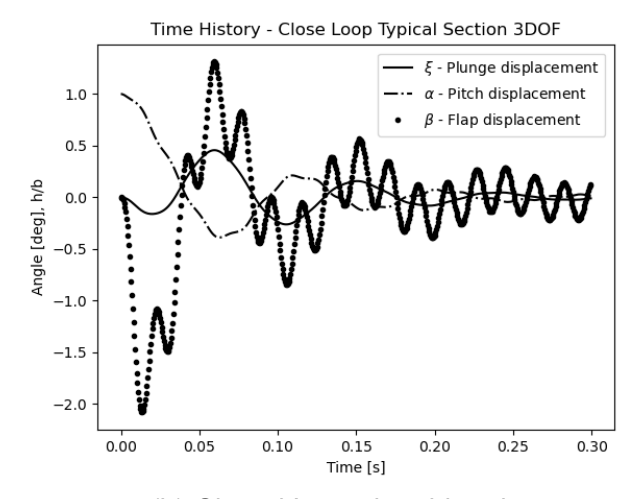
Figure 9 – Open vs closed loop root locus for a three degree of freedom airfoil employing potential theory.

Figure 10 shows simulations in time of the typical section subject to an initial displacement on the angle of attack of 1 deg. at $U/b\omega_{\alpha}=3.25$. The effect of the controller is evident by a comparison between the open and closed loop traces of the plunge (ξ) and pitch (α) DOFs responses. Whereas on the open loop simulation they are divergent, in the closed loop analysis the control surface (β), or flap, acts effectively to stabilize the system. These results obtained with the potential theory will be used on the validation of the methodology employed in this work for subsonic Mach numbers.

4. Concluding Remarks

This work presented the theoretical development of an aeroservoelastic analysis for an airfoil typical section with three degrees of freedom: pitch, plunge and trailing edge control surface deflection. The work highlighted the limitations of the rigid mesh displacement approach to compute the aerodynamic response of the disturbed flow due to the impossibility of applying this methodology for the control surface response. The implementation in the research group of the RBF approach to compute mesh displacements is validated. The paper also demonstrates the linear character of the aerodynamic response to the control surface inputs under small displacements. Finally, the development of a control law to delay the flutter onset point is presented. The controller increases the flutter speed by 22%, when compared to the open-loop behavior of the aeroelastic system. The root-locus plots





(a) Open loop time histories.

(b) Closed Loop time histories.

Figure 10 – Open vs closed loop time histories for initial condition $\alpha = 1$ deg.

of both the open and closed loop systems are presented alongside a time simulation of an initial disturbance in pitch angle to demonstrate the control law effectiveness.

5. Acknowledgments

The authors acknowledge the support for the present work provided by Fundação de Amparo à Pesquisa do Estado de São Paulo, FAPESP, under the Research Grant No. 2013/07375-0. Partial support provided by Conselho Nacional de Desenvolvimento Científico e Tecnológico, CNPq, under the Research Grant No. 315411/2023-6 is also gratefully acknowledged.

6. Authors Email Addresses

The authors can be contacted at:

- marcusvgmuniz@gmail.com,
- j.allanantunes@gmail.com
- joaoluiz.azevedo@gmail.com.

7. Copyright Statement

The authors confirm that they, and/or their company or organization, hold copyright on all of the original material included in this paper. The authors also confirm that they have obtained permission, from the copyright holder of any third party material included in this paper, to publish it as part of their paper. The authors confirm that they give permission, or have obtained permission from the copyright holder of this paper, for the publication and distribution of this paper as part of the ICAS proceedings or as individual off-prints from the proceedings.

References

- [1] Livne, E. Aircraft Active Flutter Suppression: State of the Art and Technology Maturation Needs. *Journal of Aircraft*, Vol. 55, No. 1, pp 410–452, 2018.
- [2] Silva, R. G. A. State-space aeroelastic analysis applied to fixed-wing aircraft. *Master Thesis, Escola de Engenharia de São Carlos, Universidade de São Paulo*, 1994 (In Portuguese).
- [3] Vepa, R. Finite state modeling of aeroelastic systems. *Technical Report CR-2779*, National Aeronautics and Space Administration NASA, Stanford CA, 1977.
- [4] Edwards, J. W. Unsteady Aerodynamic Modeling and Active Aeroelastic Control. *Technical Report CR-148019*, National Aeronautics and Space Administration NASA, Stanford CA, United States, 1977.

- [5] Roger, K. L. Airplane math modeling methods for active control design. AGARD, CP-228, pp. 1–11. 1977.
- [6] Eversman, W. and Tewari, A. Consistent rational-function approximation for unsteady aerodynamics. *Journal of Aircraft*, Vol. 28, No. 9, pp 545–552, 1991.
- [7] Eversman, W. and Tewari, A. Modified exponential series approximation for the Theodorsen function. *Journal of Aircraft*, Vol. 28, No. 9, pp 553–557, 1991.
- [8] Jameson, A. and Caughey, D. A finite volume method for transonic potential flow calculations. 3rd Computational Fluid Dynamics Conference, Albuquerque NM, 1977.
- [9] Pulliam, T. H. and Steger, J. L. Implicit finite-difference simulations of three-dimensional compressible flow. *AIAA Journal*, Vol. 18, No. 2, pp 159–167, 1980.
- [10] Oliveira, L. C. A methodology for state-space aeroelastic analysis using computational aerodynamics techniques. Master's thesis, Instituto Tecnológico de Aeronáutica, São José dos Campos, Brasil, 1993 (In Portuguese).
- [11] Marques, A. N. and Azevedo, J. L. F. Application of CFD-based unsteady forces for efficient aeroelastic stability analyses. *Journal of Aircraft*, Vol. 44, No. 5, pp 1499–1512, 2007.
- [12] Lyrio, J. A. A., Azevedo, J. L. F., Rade, D. A., and Silva, R. G. Computational static aeroelastic analyses in transonic flows. *AIAA AVIATION Forum*, 2020.
- [13] Lyrio, J. A. A., Azevedo, J. L. F., Rade, D. A., and Silva, R. G. Static aeroelastic computations of wing configurations in transonic flows at high Reynolds numbers. *32nd Congress of the International Council of the Aeronautical Sciences, ICAS*, 2021.
- [14] Theodorsen, T. General theory of aerodynamic instability and the mechanism of flutter. *Technical Report TR-496*, National Advisory Committee for Aeronautics NACA, Hampton VA, 1949.
- [15] Azevedo, J. H. A. Aeroelastic studies using system identification techniques. Master's thesis, Instituto Tecnológico de Aeronáutica, São José dos Campos, Brasil, 2013.
- [16] Marques, A. N. and Azevedo, J. L. F. Numerical calculation of impulsive and indicial aerodynamic responses using computational aerodynamics techniques. *Journal of Aircraft*, Vol. 45, No. 4, pp 1112–1135, 2008.
- [17] Isermann, R. and Munchhof, M. *Identification of Dynamical Systems*. Springer-Verlag, 2009.
- [18] Muniz, M. V. G. and Azevedo, J. L. F. Guidelines on the usage of system identification techniques in aeroelastic studies. 19th Brazilian Congress of Thermal Sciences and Engineering, Bento Goncalves, RS, Brazil, 2022.
- [19] Lagarias, J. C., Reeds, J. A., Wright, M. H., and Wright, P. E. Convergence properties of the Nelder–Mead simplex method in low dimensions. *SIAM Journal on Optimization*, Vol. 9, No. 1, pp 112–147, 1998.
- [20] de Boer, A., van der Schoot, M. S., and Bijl, H. New method for mesh moving based on radial basis function interpolation. *European Conference on Computational Fluid Dynamics, TU Delft*, Netherlands, 2006.
- [21] Rendall, T. and Allen, C. Efficient mesh motion using radial basis functions with data reduction algorithms. *Journal of Computational Physics*, Vol. 228, No. 17, pp 6231–6249, 2009.
- [22] Arnold, W. F. and Laub, A. J. Generalized eigenproblem algorithms and software for algebraic Riccati equations. *Proceedings of the IEEE*, Vol. 72, pp 1746–1754, 1984.
- [23] Jones, R. T. Operational treatment of the nonuniform lift theory to airplane dynamics. *Technical Report TN-667*, National Advisory Committee for Aeronautics NACA, Hampton VA, 1938.